J. Biophoton. **2**, No. 1–2, 13–28 (2009) / **DOI** 10.1002/jbio.200810024

Journal of BIOPHOTONICS

REVIEW ARTICLE

Disease recognition by infrared and Raman spectroscopy

Christoph Krafft[*,1], *Gerald Steiner*[2], *Claudia Beleites*[1], *and Reiner Salzer*[1]

[1] Bioanalytical Chemistry, Dresden University of Technology, 01062 Dresden, Germany
[2] Clinical Sensoring and Monitoring, Medical Faculty, Dresden University of Technology, Fetscherstr. 74, 01307 Dresden, Germany

Received 29 April 2008, revised 24 June 2008, accepted 24 June 2008
Published online 28 July 2008

Key words: Raman spectroscopy, infrared spectroscopy, data classification, soft tissues, hard tissues, body fluids.

Infrared (IR) and Raman spectroscopy are emerging biophotonic tools to recognize various diseases. The current review gives an overview of the experimental techniques, data-classification algorithms and applications to assess soft tissues, hard tissues and body fluids. The methodology section presents the principles to combine vibrational spectroscopy with microscopy, lateral information and fiber-optic probes. A crucial step is the classification of spectral data by a variety of algorithms. We discuss unsupervised algorithms such as cluster analysis or principal component analysis and supervised algorithms such as linear discriminant analysis, soft independent modeling of class analogies, artificial neural networks support vector machines, Bayesian classification, partial least-squares regression and ensemble methods. The selected topics include tumors of epithelial tissue, brain tumors, prion diseases, bone diseases, atherosclerosis, kidney stones and gallstones, skin tumors, diabetes and osteoarthritis.

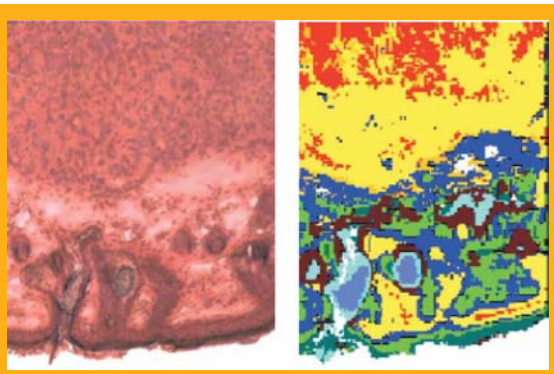

A photomicrograph of a histopathologically stained murine skin tissue section (left) is compared with a color coded FTIR image of an unstained tissue section (right). The colors allow distinguishing tumor (red, yellow, orange) and non-tumor portions.

1. Introduction

In a general sense, a disease is an abnormal condition of an organism that impairs bodily functions. Many different factors, intrinsic or extrinsic to a person, plant or animal, can cause disease. Examples of intrinsic factors are genetic defects or nutritional deficiencies. An environmental exposure, such as second-hand smoke, is an example of an extrinsic factor. Many diseases result from a combination of intrinsic and extrinsic factors. For some of them, no cause or set of causes has been identified yet. The broader body of knowledge about human diseases and their treatment is medicine. Pathology is the study and diagnosis of diseases through examination of organs, tissues, cells and bodily fluids. It can be

* Corresponding author: e-mail: christoph.krafft@ipht-jena.de

divided into anatomical pathology and clinical pathology with the latter also known as laboratory medicine. Disease diagnosis by anatomical pathology generally involves gross and microscopic visual examination of tissues with special stains employed to visualize specific proteins and other substances. Rudolf Virchow (1821–1902) is generally recognized to be the father of microscopic pathology. While the microscope had been invented earlier, Virchow was one of the first prominent physicians to emphasize the study of manifestations of disease that were visible only at the cellular level. Virchow's student Julius Cohnheim (1839–1884) combined histologic techniques with experimental manipulations, making him one of the first experimental pathologists. Cohnheim also pioneered the use of the frozen section. A version of this technique is still widely employed by modern pathologists to render diagnosis and provide other clinical information. New research techniques, such as electron microscopy, immunohistochemistry and molecular biology have expanded the means by which biomedical scientists can study disease.

Numerous developments in spectrometer and computer techniques within the past decade have enabled significant progress of IR and Raman spectroscopy in biological and life sciences. They provide a wealth of information on the cellular and molecular level from solid and liquid specimens without using external agents such as dyes, stains or radioactive labels. Their principle is that they probe molecular vibrations that depend on the composition and structure of the samples. Diseases and other pathological anomalies lead to chemical and structural changes that also change the vibrational spectra and that can be used as sensitive, phenotypic markers of the disease. Another feature which makes them attractive for modern clinical laboratories is that both methods can be automated. Recent reviews described several aspects in the field of IR and Raman spectroscopy such as biomedical applications to diagnose tissues [1], chemical imaging of biological tissue with synchrotron IR radiation [2], clinical and diagnostic applications [3], metabolic fingerprinting [4] and noninvasive biochemical analysis of single cells [5]. The progress in vibrational spectroscopy for medical diagnosis was summarized in a book that was divided into chapters about (i) the diagnosis of lymph nodes, (ii) individual human cells, (iii) micro-organisms, (iv) transmissible spongiform encephalopathy, (v) head and neck cancer, (vi) high-throughput histopathology, (vii) human cervix, (viii) esophageal and bladder, (ix) neuro-oncology and (x) erythrocytes [6]. The current review gives first an overview of the methods for data acquisition and data classification. Then frequent diseases that have been studied by Raman- and IR-based techniques are summarized, focusing on recognition of epithelial tumors, brain tumors, prion diseases, bone diseases, atherosclerosis, kidney stones and gallstones, skin tumors, diabetes and osteoarthritis.

2. Methodical overview

2.1 FTIR spectroscopy

Due to the high water content of cells, tissues and body fluids and the strong absorption of mid-IR radiation by water, the penetration depth is limited to a few micrometers. Whereas cells are sufficiently thin and fluids can be filled in cuvettes with 5 to 10 μm path length, tissue samples for most mid-IR spectroscopic studies in transmission mode are cut in 5- to 20-μm thick sections, transferred onto mid-IR transparent substrates such as calcium fluoride or barium fluoride and subsequently dried. Highly reflective, metal-coated glass slides constitute a less expensive alternative class of substrates from which IR spectra can be collected in so-called reflection absorption mode [7]. Attenuated total reflection (ATR) offers another way in IR spectroscopy to record spectra from nontransparent biomedical samples [8]. At the interface between an ATR crystal of high refractive index and the sample of lower refractive index, an evanescent wave penetrates a few micrometers into the sample. ATR crystals are made of mid-IR transparent materials such as zinc selenide, germanium, or diamond. The effective depth of penetration using the ATR principle is enhanced by multiple internal reflections. Periodic total reflections form the basis to guide radiation through optical fibers. Mid-IR transparent fibers have been fabricated using silver halides, tellurium halides and chalcogenides [9]. It has been demonstrated that uncoated fibers made of these materials can be coupled to IR spectrometers for collection of ATR spectra of aqueous body fluids such as urine [10].

Whereas most Raman spectrometers operate in a dispersive mode, mid-IR spectrometers use the interferometric Fourier-transform (FT) principle, which has the multiplex, throughput and wave number accuracy advantages. The basic setup consists of a broadband radiation source, an interferometer, a sample chamber, which can also be a microscope, and a fast detector. Many applications in microscopic pathology require the acquisition of images. The spectroscopic data can be combined with the lateral information in FTIR spectrometers with single-channel detectors by restricting radiation at the sample plane with an aperture and scanning this aperture over the area of interest with an automated translation stage. According to Abbe's law $d = 0.612\ \lambda/\mathrm{NA}$ the resolution d in spectroscopic imaging is limited by diffraction (wavelength λ and numerical aperture NA of the microscope objective). In practice, the lat-

eral resolution is often limited by the radiation from the light source rather than by the diffraction limit. To optimize the sensitivity in combination with microscope apertures near the diffraction limit, high-brilliance IR radiation from synchrotron sources is used instead of IR radiation from thermal illumination sources in standard FTIR spectrometers. As typical Cassegrain IR objectives have NA between 0.4 and 0.6, the diffraction limit is of the order of the wavelength of mid-IR radiation of 2.5 to 25 μm, which coincide with experimentally determined values [11].

FTIR spectrometers with multichannel detectors, termed focal plane array (FPA) detectors, offer another way to collect FTIR images. The entire field of view is illuminated and imaged on such an FPA detector that segments radiation at the detection plane. Without apertures and moving the samples, the lateral information is collected in parallel, whereas the spectral information is serially obtained by operating the interferometer in a special collection mode. The main advantage of FTIR spectrometers with multichannel detection is that an entire image can be acquired in a time comparable with acquiring a single spectrum conventionally. The field of view per image encompasses up to 4 mm × 4 mm, each image contains up to 4096 individual spectra and a single image can be acquired in less than a minute. As a less expensive alternative to 64 × 64 FPA detectors, 16 × 1 linear detector arrays are used to collect FTIR images by scanning this small multichannel detector over the area of interest with an automated translation stage. However, using a smaller FPA also diminishes the acquisition speed and the throughput advantage of FTIR imaging spectrometers.

2.2 *Raman spectroscopy*

The basic setup of a dispersive Raman spectrometer consists of a laser as an intense and monochromatic light source, a device that separates the elastically (Rayleigh) scattered light of the sample from the (Raman) inelastically scattered light, a spectrograph and a detector. Multichannel detectors enable registration of the whole Raman spectrum simultaneously within a fraction of a second. Due to the problem of intense autofluorescence that often masks the Raman signals, Raman spectra of unprocessed biological material are usually excited with near-IR lasers [12]. As most tissues and body fluids show minimum absorption in the wavelength interval from 700 to 900 nm, the excited autofluorescence is at a minimum, and the penetration of the exciting radiation and the scattered radiation is at a maximum. Fluorescence in Raman spectra from biological samples can also be avoided by laser excitation in the deep UV because a fluorescence-free window exists with excitation below 270 nm. However, deep-UV excitation also harbors the risk of inducing photodegradation damage. The inherent weak Raman intensities of biomolecules require the use of high-throughput optics and sensitivity-optimized detectors. Raman spectrometers are coupled to microscopes for high lateral resolution and to fiber-optic probes for remote, minimal-invasive and in-vivo applications. Because the wavelength is shorter and the NA of microscope objectives is larger, the diffraction limit of Raman microscopy is below 1 μm and higher lateral resolution can be achieved than in FTIR microscopy.

Most Raman images are collected in the point-mapping mode. Here, the laser is focused onto the sample, the scattered light is registered, and subsequently the focus or the sample is moved to the next position. In the case of laser-line illumination of the sample, the spatial data can be registered on the detector on a line parallel to the entrance slit of the spectrometer and the spectral information is dispersed perpendicularly. The second spatial dimension of an image is recorded by scanning in the direction perpendicular to that line. This so-called line-mapping registration mode is faster because only one dimension instead of two dimensions in the point-mapping mode has to be scanned. The parallel registration approaches called direct or wide-field Raman imaging employs intense, global sample illumination. The inelastically scattered light from the sample is projected onto a two-dimensional CCD detector. Most wide-field Raman imaging spectrometers use filters to select the wavelength such as dielectric, acousto-optic tunable and liquid-crystal tunable filters. Although Raman spectrometers using this principle are commercially available, applications in disease recognition have not been reported yet. The three Raman imaging modalities have been compared with respect to acquisition times, image quality, spatial resolution, intensity profiles along spatial coordinates and spectral signal-to-noise ratios [13].

In-vivo diagnostic tools are much needed in many fields of medicine such as the guidance of surgical interventions to delineate lesion margins or to replace random biopsies of suspicious tissues by targeted biopsies that, in turn, would reduce unnecessary tissue excisions, pathology costs and biopsy-associated risks. Among several optical methods currently under investigation for improvement of in-vivo endoscopic applications, such as elastic light scattering, optical coherence tomography and fluorescence spectroscopy, Raman spectroscopy offers the advantage of high molecular specificity. Several probe geometries have been designed for use with Raman spectrometers. A miniaturized probe that consisted of one central excitation fiber, six sur-

rounding collection fibers, internal in the tip filters and beveled fiber ends for optimized light collecting efficiency was designed [14] and applied in various biomedical studies [15–20]. Other Raman probes that are, however, not commercially available use 15 fibers and a ball lens [21], six fibers [22] or one fiber for signal collection [23–25]. A probe with integrated filters, one excitation and one collection fiber each from Inphotonics Inc. (USA) was recently applied to record Raman images of murine brains [26]. However, probe dimensions (13 mm diameter, 100 mm length) are probably too large for endoscopic applications. A small, unfiltered probe was suggested as an alternative, because silica with a low content of hydroxyl groups as core material shows only low spectral contributions in the high wave number region from 2400 to 3800 cm^{-1} [27]. Other new developments include the PhAT probe from Kaiser Optical Systems (USA) with global illumination and an array of 50 collection fibers [26], hollow-core photonic crystal fiber-optic probes [28] and concentric rings of optical fibers used in spatially offset Raman spectroscopy [29].

3. Supervised and unsupervised algorithms for data analysis

The main objective of classification procedures is to assign samples or data to one of a number of prior known groups or classes. Supervised approaches use reference knowledge, i.e. class membership of training data. The training process yields a model that is subsequently applied to new data and returns their class membership. If reference information is not available, the data can be grouped according to similarity. Cluster analyses belong to these so-called unsupervised approaches. If vibrational spectra are considered as a fingerprint, then the key to classify diseases based on vibrational spectroscopy is to recognize the pattern of the fingerprint. In the context of IR and Raman spectroscopy several algorithms have been applied so far that will be summarized next. In a general sense, spectral data sets can be considered as a point cloud in a multidimensional space. Simple examples of each dimension are the IR absorbance or Raman scattering intensity at a particular wave number, intensity ratios or peak widths. More complex features that can be extracted from a set of spectra as described below are principal components (PCs). A number of data points in a two-dimensional space is displayed in Figure 1. The ellipsoids in Figure 1a indicate the covariance within each class. Methods using Mahalanobis distance, principal component analysis (PCA), linear discriminant analysis (LDA) and partial least-squares regression (PLS) share the common idea to project the original data into a new coordinate system so that the covariance structures become unit matrices as shown in Figure 1b.

3.1. Mahalanobis distance

The Mahalanobis distance measures distances in units of standard deviation. Therefore, it can be used to determine the distance between a point and group or class of points. The calculation projects the data set into a new coordinate system so that the new point cloud has unit covariance, i.e. the directions are uncorrelated and have variance one. This projection is achieved by a linear combination of the origi-

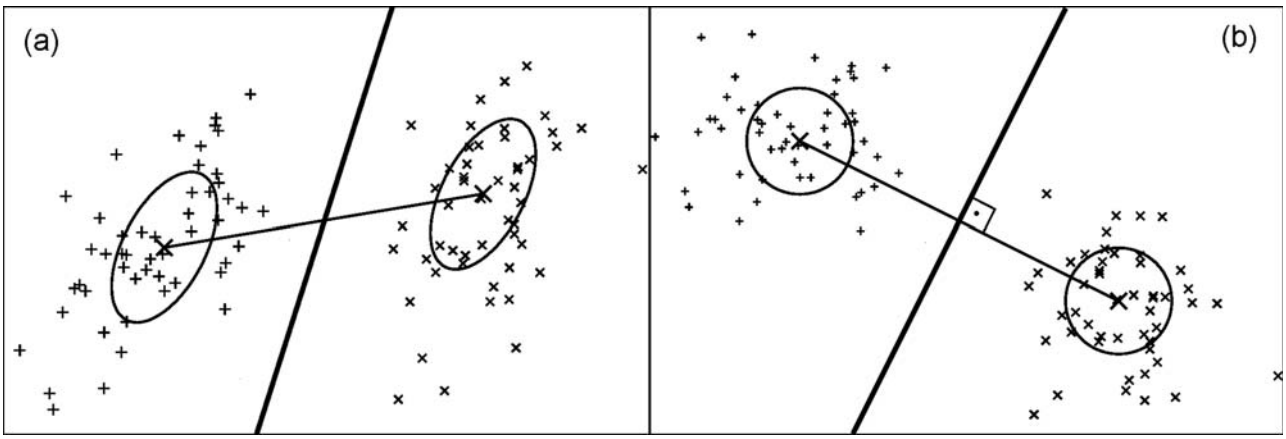

Figure 1 Principle of coordinate system transformation: **(a)** data classes (+) and (x) in original space with covariance matrices (ellipses) around class means (large X); **(b)** data set in new coordinate system with unit covariance matrices (circles) (b). The LDA discrimination plane is orthogonal to the line through the class means (b). This linear function is transformed back into the original coordinate system (a).

nal coordinate axis (e.g. the intensity or absorbance at wave numbers where the spectrum is measured). The Euclidean distance in this new coordinate system is the Mahalanobis distance.

3.2. Principal component analysis and soft independent modeling of class analogies

In principal component analysis, this projection is applied to the whole data set without any knowledge about groups. Therefore, it belongs to the unsupervised data analysis techniques. The new coordinate axes are commonly termed principal components (PCs) or loadings that are uncorrelated or orthogonal to each other. The values for each PC are called scores in the new coordinate system. PCs are ordered so that PC1 exhibits the greatest amount of variation, PC2 the second greatest amount of variation and so on. In this way PCA allows as much as possible of the variance in the data set to be described by the first significant PCs, while all subsequent PCs are so low as to be virtually negligible. For spectroscopic data, the latter PCs are dominated by noise. Therefore, PCA can be used for feature reduction [30]. Furthermore, score plots of PCA are used for visualization of data sets for skin tumors [31] and for discrimination of aorta tissues [32].

In order to build classification models according to the SIMCA algorithm (soft independent modeling of class analogies), the objects belonging to each class need to be analyzed using PCA. Only the significant PCs are retained. For a given class, the resulting model then describes either a line (for one PC), plane (for two PCs) or hyperplane (for more than two PCs). For each modeled class, the mean orthogonal distance of training data objects from the line, plane or hyperplane is used to determine a critical distance for classification. New unknown objects are projected into each PC model and the residual distance is calculated. An object is assigned to the model class when its residual distance from the model is below the statistical limit for the class. FTIR images of brain metastases have recently been assigned to the primary tumor by SIMCA [33].

3.3 Cluster analysis

In general, clustering is the partitioning of a data set into subsets (the clusters) so that the differences between the data within each cluster are minimized and the differences between clusters are maximized according to some defined distance measure. *K* means clustering groups the data set into a given number (K) of clusters. The initial centroids are randomly chosen. Then each spectrum is assigned to the cluster whose centroid is nearest. New centroids are computed, being the average of all spectra in the cluster. The two previous steps are repeated until the solution converges. The results of the *K*-means cluster analysis are the centers of each cluster and the cluster membership map. The *K*-means cluster analysis is often applied to segment IR and Raman spectra directly [26]. But scores of PCA-transformed IR [35] and Raman data sets [36] can also be used as input.

The hierarchical cluster analysis (HCA) calculates the symmetric distance matrix (size $n \times n$) between all considered spectra (number n) as a measure of their pairwise similarity. The algorithm then searches for the minimum distance, collects the two most similar spectra into a first cluster and recalculates spectral distances between all remaining spectra and the first cluster. In the next step the algorithm performs a new search for the most similar objects that now can be spectra or clusters. This iterative process is repeated $n-1$ times until all spectra have been merged into one cluster. The result is displayed in a tree-like, two-dimensional dendrogram in which one axis refers to the reduction of clusters with increasing number of iterations and the other axis to the respective spectral distances. Both clustering algorithms were compared with fuzzy C-means clustering, which is a third, less frequently used clustering algorithm, in the context of FTIR imaging of colorectal adenocarcinoma [37]. HCA are applied directly to spectra or to cluster centroids, which can be obtained by *K*-means or fuzzy clustering. The latter was used to segment FTIR images of cervical cancer [38].

3.4 Linear discriminant analysis

A number of objects belong exactly to one out of k similar classes and the class membership is known for each object. Each object is defined by characteristic parameters. LDA uses this information to calculate $(k-1)$ linear discriminant functions that optimally discriminate k classes. LDA uses these functions to assign unknown objects to classes. The discriminant functions describe a separation hyperplane. The normal vector of this separation plane is the direction that maximizes the ratio of the difference between classes (interclass variance) to the differences within the classes (intraclass variance). This direction of the vector is simply the direction that connects the class means if the intraclass variance is one in all directions, i.e. if the intraclass covariance matrix is the unity matrix (compare Figure 1b). LDA classification is based on the Mahalanobis distance that is derived

from a common covariance matrix for all classes, while quadratic discriminant analysis (QDA) classification is based on a Mahalanobis distance that is based on class-specific covariance matrices.

LDA using spectral band ratios as parameters was applied to distinguish FTIR images of normal brain tissue and primary brain tumors [39] and FTIR images of normal brain tissue and brain metastases originating from different primary tumors [40]. LDA using PCs as input was applied to identify Raman spectra of epithelial tumors [16, 41, 42]. LDA and QDA based on optimally selected spectral regions were compared to classify IR spectra of exfoliated cervical cell specimens [43].

3.5 Partial least-squares regression

PCA, LDA, and PLS use a common transformation principle that is based on calculation of the Mahalanobis distance. Whereas LDA is the supervised classification analogue to PCA, PLS is the supervised regression analogue. PLS regression is based on factorization of matrices, which can be performed by PCA. PLS models are developed for the independent variables (e.g. concentration) as well as for the dependent variables (e.g. absorbance) based on PCs. Both results constitute the external relations. An internal relation realizes a correlation between independent and dependent variables. PLS regression models were developed for quantitative analysis of serum by Raman spectroscopy [44] and body fluids by IR spectroscopy [45].

3.6 Artificial neural networks

ANNs offer a flexible way to model nonlinear functions. Backpropagation ANNs are constructed with a layered structure in which each node is connected to all nodes of the previous and the next layer with different weights. The input layer (a node for each wavelength or feature) and the output layer (one node per class) are commonly connected by a single hidden layer. The input to each node is the linear combination of the outputs of the previous layer using the respective weights for the connections. Each node consists of an activation function that is most commonly of sigmoid or Gaussian shape. The output of the node is the result of the activation function for the input value. ANNs were used with extended spectral ranges as well as PCs to identify lesions in breast tissue [46]. ANN using a three-layer feed forward network [47] and ANN using top level and sublevel networks [48] identified scrapie infection from IR spectra of blood serum.

3.7 Bayes rule

Bayes classification rule is based on the use of a learning algorithm and a probabilistic determination to relate a small number of spectral metrics to specific histologic entities. According to the Bayes rule a sample should be assigned to the class that is most likely given the particular observation (i.e. the spectrum). As a prerequisite the conditional probabilities of the classes need to be known. These probabilities might be directly estimated from the distribution of the data along the used features. Bayesian classification has been suggested for high-throughput assessment of FTIR images from prostate tissue [49, 50].

3.8 Support vector machines

SVM use spectra close to the class borders as support vectors to define the discriminant surface. SVM enlarge the feature space so that nonlinear class boundaries (in the original feature space) can be modeled. SVM were applied as a member of ensemble methods for the identification of bovine spongiform encephalopathy by IR spectra of serum [51].

3.9 Ensemble methods

If the classifiers lack stability, models can be improved by ensemble methods, a process that is also known as aggregation. The idea is to combine the predictions of a number of different classifiers into a new prediction. LDA, PCA-based LDA, SVM and ANN were averaged to obtain a classification result for BSE by IR spectra of serum [51]. Another way to form an ensemble of models for aggregation uses the same method, but with slight variations of training data. This principle was demonstrated for LDA classification of FTIR images from brain tumors in small sample size situations [52]. A combination of the output of different classification methods (PLS, LDA, principal component regression, ridge regression) also including aggregated decision trees (random forest model) were applied to identify BSE by IR spectra of serum [53].

4 Selected applications

4.1 Tumors of epithelial tissue

Epithelium is the collective term for cover and glandular tissue. It is composed of layers of cells that line the outside and inside surfaces of organs. As the

epithelium covers the surface of organs it is exposed to the environment and is in contact with a broad range of potentially aggressive or harmful chemical and physical conditions that can induce a deregulation of cells division. Therefore, tumors of the epithelium – usually called carcinomas – are among the most common forms of cancer. FTIR and Raman studies included carcinomas of the prostate, cervix uteri, skin, breast, colon, esophagus, bladder and oral mucosa.

Prostate carcinoma was selected as an application to demonstrate that a combination of FTIR imaging, tissue microarrays and fast numerical analysis enables rapid histopathological recognition [49, 50, 54]. FTIR imaging permits rapid recording of data from large numbers of tissue samples. Tissue microarrays consist of multiple tissue samples of uniform dimensions placed on a single substrate. This arrangement facilitates identical processing for all samples after constructing the array. Arrays of 12×8 biopsies with 500 μm diameter were prepared. High-throughput assessment of tissue sections was achieved in these studies by a metric Bayes classification.

One field of research that has received substantial attention in the last decade was the application of FTIR and Raman spectroscopy to gynecological screening for cervical dysplasia and malignancies [reviews: 55–57]. Dysplasia is a term used in pathology to refer to an abnormality in maturation of cells within a tissue. It is often indicative for an early neoplastic process. The currently accepted technique for diagnosing exfoliated cells is the Papanicolaou (Pap) smear test where cells are collected from the cervical transformation zone and stained with the Pap stain. Despite its success, cytological screening by the Pap smear test has limitations, the most important being high numbers of false-negative results. Therefore, since the pioneering work by Wong and coworkers in the early 1990s [58], the main objective has been to improve the diagnostic accuracy of the Pap smear by FTIR spectroscopy of exfoliated cervical cells [43]. The focus of the Raman spectroscopic research on cervical tissue was in-vivo assessment of squamous dysplasia by fiber-optic probes [24]. Cervical tissue sections have been studied independently by three groups using FTIR imaging [38, 59, 60].

Whereas tissue sections are prepared for IR spectroscopy, biopsy blocks of epithelial tissues, precancers and cancers from the larynx, tonsil, oesophagus, stomach, bladder and prostate could be studied by near-infrared Raman spectroscopy [41, 42, 61]. Data were classified by principal-component-fed linear discriminant models.

Epithelial tissue such as oesophagus and oral mucosa was also a target to collect Raman spectra by fiber-optic probes. Raman spectra of the rat esophagus were collected ex-vivo with three different fiber-optic probes in order to mimic instrument calibration, probe-to-probe and day-to-day variations [18]. Raman spectra of the rat palate were collected even under in-vivo conditions [16]. Dysplasia in the epithelium of the rat palate was induced by topical application of a carcinogen.

4.2 Brain tumors and neurodegenerative diseases

There are at least 1000 diseases that can affect the nervous system, and approximately one in three people will be affected by one of them at some point in life. The seriousness of these diseases has led to a large emphasis on research into their causes, diagnoses, therapies and prevention. In the context of brain tissue, IR and Raman spectroscopy were applied to primary brain tumors, secondary brain tumors [62] and neurodegenerative diseases that are induced by prions [63].

Whereas primary brain tumors originate from cells within the brain, secondary brain tumors are metastases from primary tumors outside the brain. Two classification models were developed to determine the primary tumor of brain metastases based on FTIR imaging [34, 40]. The first model extracted nine variables from IR training spectra and used the algorithm linear discriminant analysis (LDA) to assign test spectra. The second model performed a principal component analysis from FTIR training images and used the algorithm soft independent modeling of class analogies to assign FTIR images. Another LDA model required only three variables to recognize FTIR images of malignant gliomas, the most frequent primary brain tumors [39].

Brain tumors can be induced in rats and mice by injection of tumors cells directly into the brain or into the carotid artery. Tissue samples from these animal models were studied by IR spectroscopy [35, 64] and Raman spectroscopy [26, 36]. Raman images were collected from brain-tissue blocks using a fiber-optic probe and a motorized stage [26]. Figure 2 shows photographs, Raman images and Raman spectra that were collected from nondried tissues with the same system. Normal brain tissue can clearly be distinguished from a brain metastasis of lung cancer by different spectral contributions due to protein, lipids, water, hemoglobin and carotene. Brain metastases of malignant melanomas were sensitively detected because the spectral contributions of the pigment melanin were resonance enhanced [26].

FTIR microspectroscopy of prion diseases has been recently reviewed [65, 66]. This method was proposed to identify prion-affected nervous cells or tissues due to its ability to detect localized changes in structure and composition of disease-associated prion protein PrP^{sc}. It was illustrated on how the ap-

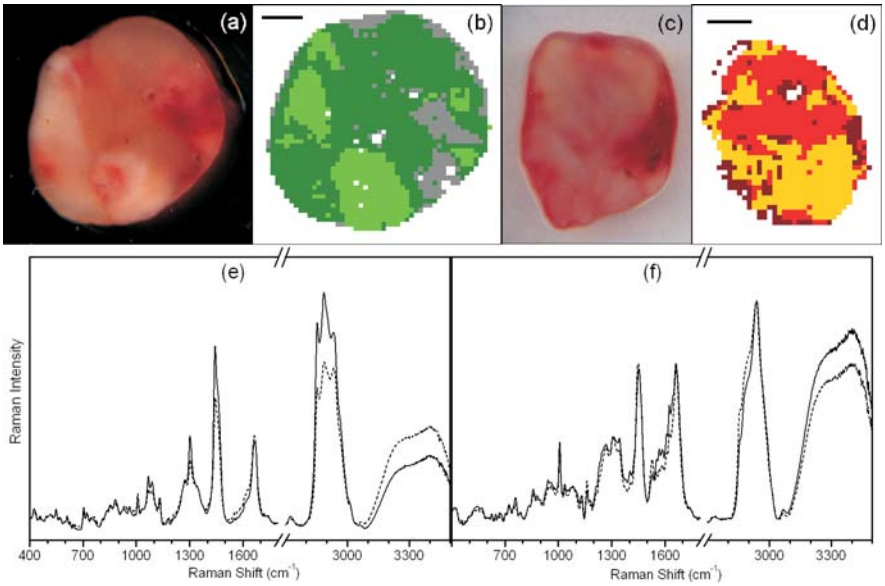

Figure 2 (online colour at: www.biophotonics-journal.org) Photographs and Raman imaging of non-dried normal brain tissue **(a, b)** and a brain metastasis of lung cancer **(c, d)**. Raman images were segmented into three clusters by *k*-means cluster analyses. Raman spectra of the light green (solid in **(e)**), dark green (dashed in (e)), red (solid in **(f)**) and orange clusters (dashed in (f)). Spectral contributions due to proteins, lipids, hemoglobin, carotene and water differ throughout the spectra.

plication of brilliant IR synchrotron light sources can improve the lateral resolution and subsequently the detection limit in the context of prion diseases [67].

Prion disease was identified antemortem in bovine spongiform encephalopathy (BSE) infected cattle [51, 68] and hamsters [47, 48] by a combination of IR spectra from sera and advanced methods of pattern recognition. The experimental findings indicated the presence of distinct surrogate markers in the sera rather than the direct detection of the pathological prion protein. Spectral features that were selected based on the calculation of the covariance of the spectral points were used as input for the artificial neural network (ANN) classification [47]. Another approach selected features based on a stochastic search and optimization algorithm – a so-called genetic algorithm. The 20 most suitable features were used for classification by linear or quadratic discriminant analysis [68]. An approach called diagnostic pattern recognition (DPR) combined four mathematical classification approaches (principal component analysis plus linear discriminant analysis, robust linear discriminant analysis, artificial neural network and support vector machine). DPR-analysis of IR spectra confirmed the reliable assignment to the classes BSE-positive or BSE-negative [51].

4.3 Bone diseases

Mineralized biological samples are composed of an inorganic matrix (calciumphosphate) and an organic matrix consisting predominantly of collagen type 1 and cells. The use of IR spectroscopy, microspectroscopy and microspectroscopic imaging to probe the composition and physicochemical status of mineral and matrix of bone in health and disease has been reviewed [69]. In contrast to conventional histological techniques, vibrational spectroscopic methods do not require a special sample preparation, e.g. homogenization, decalcification, extraction or dilution. They enable investigation of hard tissue under native conditions. IR studies of bone-related diseases include osteoporosis [70, 71] and osteomalacia [72]. In osteoporosis the bone mineral density is reduced, bone microarchitecture is disrupted and the amount and variety of noncollagenous proteins in bone is altered that all lead to an increased risk of fracture. Osteomalacia is the general term for the softening of the bone due to defective bone mineralization. Many of the effects of the disease overlap with the more common osteoporosis, but the two diseases are significantly different. Raman spectroscopy was applied to craniosynostosis [73, 74], which is an abnormal condition of bones making up the skull. Recently, the first transcutaneous Raman spectrum of human bone in vivo has been obtained at skin-safe laser illumination levels using spatially offset Raman spectroscopy [30]. This technique, which is based on collecting Raman spectra away from the point of laser illumination using concentric rings of optical fibers, provides chemically specific information on deep layers of human tissue well beyond the reach of existing comparative approaches. Microdamages in bone were investigated both by FTIR imaging [75] and Raman imaging [76]. Another interesting application of Raman spectroscopy is the detection of dental caries in teeth. While optical coherence tomography was used to screen carious sites and to determine lesion depth, fiber-optical Raman spectroscopy provided biochemical confirmation of caries [77].

4.4 Atherosclerosis

Atherosclerosis is a disease affecting arterial blood vessels. The atherosclerotic plaque is divided into (i) the atheroma that is composed of macrophages nearest the lumen of the artery, (ii) underlying areas of cholesterol crystals, and (iii) calcification at the outer base of older and more advanced lesions, respectively. Previous research has suggested that the microscopic morphology and chemical composition rather than the anatomy of an atherosclerotic plaque determine plaque stability and disease progression. For this reason, FTIR spectroscopy was applied to obtain both chemical and spatial information on the distribution of different components within atherosclerotic arteries. Whereas one study [78] examined atherosclerotic human artery under moist conditions, other studies detected the calcification in thin dried sections of rabbit aortas both in transmission mode [79–81] and micro-ATR reflection mode [82].

Developments of compact clinical Raman systems, specially developed Raman catheters and future directions of Raman spectroscopy in cardiovascular medicine have been summarized [83]. The performance of a fiber-optic probe was tested in vitro with aorta tissue [21]. Raman maps of human atherosclerotic plaques were generated to investigate the chemical composition of the pigment ceroid in cross sections of the intimal surface [84] and to investigate plaque development in mice [85]. Compact clinical Raman systems and dedicated, miniaturized fiber-optic Raman catheters with a side-viewing geometry were used ex vivo in human coronary arteries [86] and in vivo in lambs and sheep to illuminate the blood vessel wall and to collect Raman scattered light [17]. The in-vivo intravascular Raman signal obtained from a blood vessel was found to be a simple summation of signal contributions of the blood vessel wall and of blood. Therefore, algorithms previously developed from single-point Raman spectra [87] could be adapted to extract information about the chemical composition of blood vessel walls from in-vivo Raman spectra.

4.5 Kidney stones and gallstones

Kidney stones and gallstones are common diseases worldwide. Approximately 5% of the population will suffer from kidney stones at some point in their life. 10 to 15% of the population carries gallstones that stay asymptomatic in most cases (ca. 75%). About 70% of all kidney stones are composed of calcium oxalate, and small amounts of calcium hydroxyapatite, uric acid and magnesium ammonium phosphate. Other types of stones consist of 50% hydroxyapatite or calcium monohydrogen phosphate or are composed of cystine. Gallstones are commonly classified into three classes: cholesterol (white), pigment (black) and mixed (brown) stones. Each type of stones has its own treatment regimens. Determination of composition is one fundamental part in establishing the cause and likelihood of recurrence of stones, as well as an appropriate treatment. Few Raman spectroscopic studies on gallstones [88, 89] and kidney stones [90–92] and many IR spectroscopic studies on gallstones [93, 94] and kidney stones [95–97] demonstrated that vibrational spectroscopy delivers useful information on the stones structure and composition. The investigation is direct, fast, and nondestructive, and does not require tedious sample preparation. There are at least two approaches to the quantitative analysis of the stone composition. PLS techniques will yield highly precise results if the composition of the unknown material is restricted to a reasonably well-defined range, with predictable components present. Another approach is based on supervised methods or on library searching. An unknown sample spectrum is then compared to a number of well-assigned library spectra and the best correlated spectrum is found. In particular, Raman spectroscopy is well suited to detect phosphate-type kidney stones because the main constituent hydroxyapatite has a distinctive line at 961 cm^{-1} that can be used as a marker band. Although most reports in the literature are aimed on the investigations of gallstones from adults the analysis of children is important as well due to the growing number of cases. Recently, it was demonstrated by IR spectroscopy that the composition of black and brown stones from both children and adults are similar [98]. Surprisingly, the results suggest that the risk factors and the mechanism responsible for stone formation might also be the same in both children and adults.

4.6 Skin tumors

Skin tumors that include squamous cell carcinoma, malignant melanoma and basal cell carcinoma (BCC), are the cancers with the highest incidence worldwide. Understanding the molecular, cellular and tissue changes that occur during skin carcinogenesis is central to cancer research in dermatology. As for many other tissues, vibrational spectroscopy has been used to evaluate these changes [review: 99]. An example of skin tissue characterization by FTIR imaging is shown in Figure 3. Beside the clear classification of the tumor in the top part, the detection of tumor within connective tissue is particular impressive, since these tumor cells are usually difficult to identify in the stained tissue section. BCC is the most common cancer of the skin. Raman images

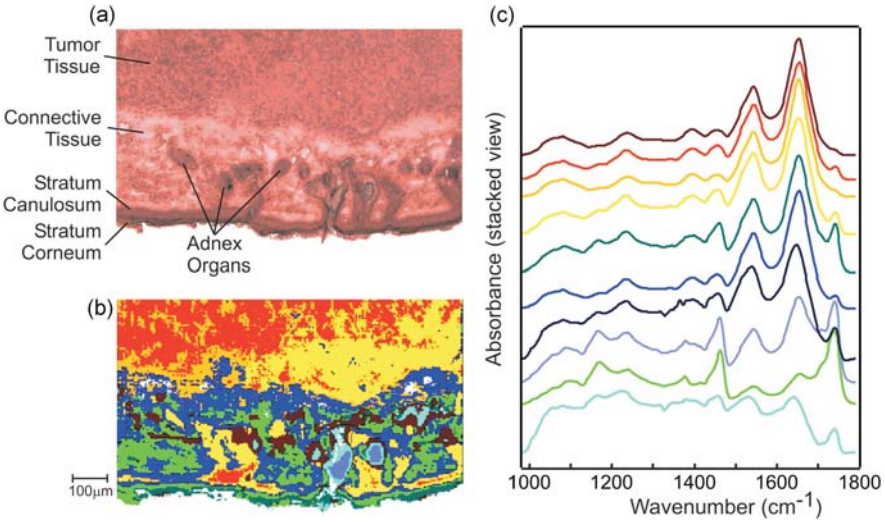

Figure 3 (online colour at: www.biophotonics-journal.org) Hematoxylin-eosin stained murine skin tissue section **(a)**. The FTIR image of this section before staining consists of more than 65 000 spectra **(b)**. The colors represent the class membership of a fuzzy-cluster analysis (b). IR spectra averaged from each cluster **(c)**. Same color code in (b) and (c): tumor = red, yellow and orange; connective tissue = green and blue; adnex organs = brown, skin layers = dark green.

were acquired form fifteen sections of BCC and compared with histopathology [100]. In this sample set, 100% sensitivity and 93% selectivity were demonstrated. Pigmented levi, which belong to benign skin lesions, were distinguished from malignant skin lesions in thin sections of biopsies by FTIR imaging [101]. Melanoma is the most aggressive skin cancer and is invariably fatal if left untreated. Melanoma removal at an early stage is almost always curative, leading to a good prognosis for the patient. Melanoma, pigmented nevi, BCC, seborrheic keratoses and normal skin were studied by Raman spectroscopy [102]. The sensitivity and specificity of an artificial neural network classification for diagnosis of melanoma were 85% and 99%, respectively. IR spectroscopy was used to explore distinctive characteristics of BCC versus normal skin samples and other skin neoplasms such as squamous cell carcinoma, nevi and malignant melanoma [103]. This study combined LDA with a routine to optimally select wave-number regions for classification. Recently it was demonstrated that micro-Raman imaging is also well suitable to distinguish between normal and malignant skin cells at a subcellular level [104]. The Raman scattering was excited at 633 and 515 nm. An excitation power of less than 2 mW ensures that cells were not damaged. The potential of Raman spectroscopy as a tool for skin studies is now being realized by dedicated spectrometers which three groups have independently developed [105, River Diagnostics NL, Pharmanex USA].

4.7 Diabetes

The IR-based analytical method for consideration as clinical assay is a field that has been pioneered by Mantsch and coworkers [106]. Recent reviews also included Raman-based techniques in this field [4, 107]. A number of common clinical chemistry tests have proven to be feasible using these approaches. Among the most important applications is the fast and reliable determination of the glucose level in the blood of diabetes patients. Normally, the glucose level is tightly regulated in the human body. Failure to maintain blood glucose in the normal range between 70 and 150 mg/dL leads to conditions of persistently high (hyperglycemia) or low (hypoglycemia) blood sugar. Diabetes mellitus, which is characterized by persistent hyperglycemia of several causes, is the most prominent disease related to failure of blood-sugar regulation. A spectroscopic method based on ATR-FTIR spectroscopy has been developed for reagent-free analysis of blood and urine constituents [45]. Blood plasma, whole blood and urine were analyzed in sample volumes as small as 5 µL without any sample preparation such as drying or enrichment. Partial least-squares regression was used as a mathematical model to construct a prediction model that could calculate the concentration of glucose, the protein albumin, total protein, cholesterol, urea and triglycerides in whole blood or blood plasma samples, and the concentration of urea, uric acid, phosphate and creatinine in urine samples. The absolute precision and reproducibility of the prediction reached was sufficient for routine clinical analysis and was only limited by the precision of the reference analysis used for calibration.

Raman spectroscopy was explored as a reagent-free tool for predicting the concentrations of different parameters in blood serum and serum ultrafiltrate [44]. In an investigation using samples from 247 blood donors the concentrations of glucose, triglycerides, urea, total protein, cholesterol, high-density lipoprotein, low-density lipoprotein and uric acid were determined with accuracy within the clinically interesting range. Furthermore, it was shown that ul-

trafiltration can efficiently reduce fluorescent light background to improve prediction accuracy such that the relative coefficient of variation decreased for glucose and urea in ultrafiltrate by more than a factor of 2 when compared to serum.

4.8 Osteoarthritis

As vibrational spectroscopy is an analytical technique that can quantify spatial and temporal changes in matrix composition, it enables characterization of degenerative cartilage diseases and the efficacy of potential therapies. Articular cartilage consists of chondrocytes cells embedded in an extracellular matrix composed predominantly of a hydrophilic proteoglycan gel enmeshed in a dense network of type-II collagen fibrils. So far, significant complications in the management of osteoarthritis, a progressively disabling disease of the joints, have been the inability to identify early cartilage changes during development of the disease and the lack of techniques to evaluate the tissue response to therapeutic and tissue-engineering interventions. A recent study elucidated several IR spectroscopic parameters that enable evaluation of molecular and compositional changes in human cartilage with osteoarthritis and in repair cartilage from animal models [108]. Degenerative cartilage was also analyzed using an IR fiber-optic probe [109]. These preliminary results suggested that it may be possible to monitor subtle changes related to early cartilage degeneration. Using an IR fiber-optic probe allows determination of cartilage integrity in situ during arthroscopy.

5. Conclusions and outlook

IR and Raman spectroscopy can be applied to a wide variety of sample morphologies such as thin sections, native tissue, soft tissue, hard tissue and body fluids. The main advantage of IR spectroscopy is a shorter acquisition time of spectra due to the interferometric Fourier transform principle that is utilized in combination with multichannel detectors for rapid acquisition of images. Due to the signal enhancement, coherent anti-Stokes Raman spectroscopy (CARS) in combination with fast scanning mirrors offers the perspective to reduce the acquisition time of Raman images. CARS imaging with video-rate microscopy of skin tissue in a live mouse at subcellular resolution has already successfully been performed [110]. The main advantage of Raman spectroscopy is the ability to obtain spectra of aqueous samples because the Raman signals of water are weak. Multireflective attenuated total reflection (ATR) sample cells have been developed to collect IR spectra also from aqueous solutions. With the ongoing progress in light sources, optical components, detectors and algorithms for data processing, the number of applications of vibrational spectroscopy in disease recognition will increase in the future. We are optimistic that IR and Raman spectroscopic based methods will soon become important clinical tools that complement the standard techniques in various fields of disease recognition.

Christoph Krafft received his Diploma in physics from the University of Oldenburg, Germany, in 1994 and his Ph.D. in biophysics on Raman spectroscopy of protein–DNA interaction from the Humboldt University Berlin, Germany in 1998. From 1998–2000, he was a Postdoc in the group of Prof. G. J. Thomas Jr. at the University of Missouri, Kansas City, USA, studying biological macromolecules by Raman spectroscopy. From 2000–2006 he was a leader of a junior research group at the University of Technology, Dresden, Germany, working on FTIR and Raman imaging of tissues and cells. In 2007, he joined the group of Prof. V. Sergo (University of Trieste, Italy) as a research associate applying FTIR and Raman imaging to congenital malformations of lung and colon. In 2007, he received his habilitation at the Dresden University of Technology where he joined as a research associate in 2008 working on tumor diagnosis in living mice by Raman spectroscopy. Since June 2008, Dr. Krafft is a research group leader at the Institute for Photonic Technology (Jena, Germany) working on optical cell identification. He is the author of about 40 scientific papers including reviews and contributions to books about bioanalytical applications of vibrational spectroscopies.

Reiner Salzer received his Ph.D. on IR band intensities at the University of Leipzig, Germany in 1971 where he also received his Habilitation in 1979. In 1990/91 he worked as Visiting Professor at the Chemical Institute of the University of Oslo, Norway. In 1990, he became Professor of Analytical Chemistry at the University of Technology in Dresden, Germany. In 1997, he became a Member of The Norwegian Academy of Science and Letters. He was Chairman (elected) of the GDCh (Ge-

sellschaft Deutscher Chemiker) Division Analytical Chemistry from 2000–2003 and since 2003, he is Head of the Study Group Education of DAC/EuCheMS. In 2007, Dr. Salzer received the Emich Plaque of the Austrian Society of Analytical Chemistry. His scientific interests include molecular monitoring for early diagnosis of diseases, polymers with biologically active functions, and electronic media in university education. He is the author of 5 books, about 210 publications, and has 15 patents.

Claudia Beleites studied chemistry at Justus Liebig University, Gießen, Germany from 1997–2000, and from 2000–2003 at the University of Technology, Dresden, Germany. In 2003 she received her Diploma in chemistry. From 2003–2004, she spent 6 months at the Institute for Biodiagnostics (National Research Council Canada) in Winnipeg, Canada. From 2004–2008 she did PhD studies at Dresden University of Technology, Dresden Germany on the topic of Raman spectroscopic brain tumor diagnosis and chemometric data analysis. Since 2008, she is a research associate in the group of Prof. V. Sergo (University of Trieste, Italy) applying Raman spectroscopy for tissue diagnosis.

Gerald Steiner studied biomedical engineering at the University of Technology in Dresden, Germany and received his Ph.D. degree in 1993. After working in the device-making industry he returned to the University of Technology, Institute for Analytical Chemistry, in 1994. He worked in research and development in the field of fiber-optical sensors and biosensor arrays with label-free optical detection. He spent a postdoc position at the National Research Council, Institute for Biodiagnostics, in Winnipeg, Canada. After 12 years research experience in biosensing and optical spectroscopy he joined the Medical Faculty of the University of Technology in Dresden and is working now in the field of optical imaging spectroscopy and multimodal imaging in medicine.

References

[1] C. Krafft and V. Sergo, Biomedical applications of Raman and infrared spectroscopy to diagnose tissues. Spectroscopy **20**, 195–218 (2006).
[2] L. M. Miller and P. Dumas, Chemical imaging of biological tissue with synchrotron infrared light. Biochem. Biophys. Acta **1758**, 846–857 (2006).
[3] J. Dubois and R. A. Shaw, IR spectroscopy in clinical and diagnostic applications. Anal. Chem. **76**, 360A–367A (2004).
[4] D. I. Ellis and R. Goodacre, Metabolic fingerprinting in disease diagnosis: biomedical applications of infrared and Raman spectroscopy. Analyst **131**, 875–885 (2006).
[5] R. J. Swain and M. M. Stevens, Raman microspectroscopy for non-invasive biochemical analysis of single cells. Biochem. Soc. Trans. **35**, 544–549 (2007).
[6] M. Diem, J. M. Chalmers, and P. R. Griffiths (eds.) Vibrational Spectroscopy for Medical Diagnosis, (John Wiley & Sons Ltd, Chichester, 2008).
[7] M. Diem, M. Romeo, S. Boydston-White, M. Miljkovic, and C. Matthäus, A decade of vibrational microspectroscopy of human cells and tissue (1994–2004). Analyst **129**, 880–885 (2004).
[8] S. G. Kazarian and K. L. A. Chan, Applications of ATR-FTIR spectroscopic imaging to biomedical samples. Biochim. Biophys. Acta **1758**, 858–867 (2006).
[9] B. Mizaikoff, Mid-IR fiber-optic sensors. Anal. Chem. **75**, 258A–267A (2003).
[10] S. Cytron, S. Kravchick, B. A. Sela, E. Shulzinger, I. Vasserman, Y. Raichlin, and A. Katzir, Fiber-optic infrared spectroscopy: a novel tool for the analysis of urine and urinary salts in situ and in real time. Urology **61**, 231–235 (2003).
[11] P. Lasch and D. Naumann, Spatial resolution in infrared microspectroscopic imaging of tissues. Biochim. Biophys. Acta **1758**, 814–829 (2006).
[12] C. Krafft, Bioanalytical applications of Raman spectroscopy. Anal. Bioanal. Chem. **378**, 60–62 (2004).
[13] S. Schlücker, M. D. Schaeberle, S. W. Huffmann, and I. W. Levin, Raman microspectroscopy: a comparison of point, line, and wide-field imaging methodologies. Anal. Chem. **75**, 4312–4318 (2003).
[14] M. G. Shim, B. C. Wilson, E. Marple, and M. Wach, Study of fiber-optic probes for in vivo medical Raman spectroscopy. Appl. Spectrosc. **53**, 619–627 (1999).
[15] M. G. Shim, L. M. Wong Kee Song, N. E. Marcon, and B. C. Wilson, In vivo near-infrared Raman spectroscopy: demonstration of feasibility during clinical gastrointestinal endoscopy. Photochem. Photobiol. **72**, 146–150 (2000).
[16] T. C. Bakker Schut, M. J. H. Witjes, H. J. C. M. Sterenborg, O. C. Speelman, J. L. N. Roodenburg, E. T. Marple, H. A. Bruining, and G. J. Puppels, In vivo detection of dysplastic tissue by Raman spectroscopy. Anal. Chem. **72**, 6010–6018 (2000).
[17] H. P. Buschmann, E. T. Marple, M. L. Wach, B. Bennet, T. C. Bakker Schut, H. A. Bruining, A. V.

Bruschke, A. van der Laarse, and G. J. Puppels, In vivo determination of the molecular composition of artery wall by intravascular Raman spectroscopy. Anal. Chem. **72**, 3771–3775 (2000).

[18] I. A. Boere, T. C. Bakker Schut, J. van den Boogert, R. W. F. de Bruin, and G. J. Puppels, Use of fiber-optic probes for detection of Barrett's epithelium in the rat oesophagus by Raman spectroscopy. Vib. Spectrosc. **32**, 47–55 (2003).

[19] L. M. Molckovsky, Wong Kee Song, M. G. Shim, N. E. Marcon, and B. C. Wilson, Diagnostic potential of near-infrared Raman spectroscopy in the colon: differentiating adenomatous from hyperplastic polyps. Gastrointest. Endosc. **57**, 396–402 (2003).

[20] P. Crow, A. Molckovsky, N. Stone, J. Uff, B. Wilson, and L. M. Wong Kee Song, Assessment of fiber-optic near infrared Raman spectroscopy for diagnosis of bladder and prostate cancer. Urology **65**, 1126–1130 (2005).

[21] J. T. Motz, M. Hunter, L. H. Galindo, J. A. Gardecki, J. R. Kramer, R. R. Dasari, and M. S. Feld, Optical fiber-probe for biomedical Raman spectroscopy. Appl. Optics **43**, 542–554 (2004).

[22] C. J. Barbosa, F. H. Vaillancourt, L. D. Eltis, M. W. Blades, and R. F. B. Turner, The power distribution advantage of fiber-optic coupled ultraviolet resonance Raman spectroscopy for bioanalytical and biomedical applications. J. Raman Spectrosc. **33**, 503–510 (2002).

[23] A. Mahadevan-Jansen, M. F. Mitchell, N. Ramanujam, U. Utzinger, and R. Richards-Kortum, Development of a fiber-optic probe to measure NIR Raman spectra of cervical tissue in vivo. Photochem. Photobiol. **68**, 427–431 (1998).

[24] U. Utzinger, D. L. Heintzelman, A. Mahadevan-Jansen, A. Malpica, M. Follen, and R. Richards-Kortum, Near-infrared Raman spectroscopy for in vivo detection of cervical precancers. Appl. Spectrosc. **55**, 955–959 (2001).

[25] Z. Huang, H. Zeng, I. Hamzavi, D. McLean, and H. Lui, Rapid near-infrared Raman spectroscopy system for real-time in vivo skin measurements. Opt. Lett. **26**, 1782–1784 (2001).

[26] C. Krafft, M. Kirsch, C. Beleites, G. Schackert, and R. Salzer, Methodology for fiber-optic Raman mapping and FTIR imaging of metastases in mouse brains. Anal. Bioanal. Chem. **389**, 1133–1142 (2007).

[27] L. F. Santos, R. Wolthuis, S. Koljenovic, R. M. Almeida, and G. J. Puppels, Fiber-optic probes for in vivo Raman spectroscopy in the high-wave number region. Anal. Chem. **77**, 6747–6752 (2005).

[28] M. V. Schulmerich, W. F. Finney, R. A. Fredricks, and M. D. Morris, Subsurface Raman spectroscopy and mapping using a globally illuminated non-confocal fiber-optic array probe in the presence of Raman photon migration. Appl. Spectrosc. **60**, 109–114 (2006).

[29] S. O. Konorov, C. J. Addison, H. G. Schulze, R. F. Turner, and M. W. Blades, Hollow-core photonic crystal fiber-optic probes for Raman spectroscopy. Opt. Lett. **31**, 1911–1913 (2006).

[30] P. Matousek, E. R. Draper, A. E. Goodship, I. P. Clark, K. L. Ronayne, and A. W. Parker, Noninvasive Raman spectroscopy of human tissue in vivo. Appl. Spectrosc. **60**, 758–763 (2006).

[31] N. Uzunbajakava, A. Lenferink, Y. Kraan, E. Volokhina, G. Vrensen, J. Greve, and C. Otto, Nonresonant confocal Raman imaging of DNA and protein distribution in apoptotic cells. Biophys. J. **84**, 3968–3981 (2002).

[32] P. Lasch and D. Naumann, FTIR microspectroscopic imaging of human carcinoma in thin sections based on pattern recognition techniques. Cell. Mol. Biol. **44**, 189–202 (1998).

[33] F. Bonnier, S. Rubin, L. Venteo, C. M. Krishna, M. Pluot, B. Baehrel, M. Manfait, and G. D. Sockalingum, In-vitro analysis of normal and aneurismal human ascending aortic tissue using FTIR microspectroscopy. Biochim. Biophys. Acta **1758**, 968–973 (2006).

[34] C. Krafft, L. Shapoval, S. B. Sobottka, K. D. Geiger, G. Schackert, and R. Salzer, Identification of primary tumors of brain metastases by SIMCA classification of IR spectroscopic images. Biochim. Biophys. Acta **1758**, 883–891 (2006).

[35] N. Amharref, A. Beljebbar, S. Dukic, L. Venteo, L. Schneider, M. Pluot, R. Vistelle, and M. Manfait, Brain tissue characterization by infrared imaging in a rat glioma model. Biochim. Biophys. Acta, **1758**, 892–899 (2006).

[36] N. Amharref, A. Beljebbar, S. Dukic, L. Venteo, L. Schneider, M. Pluot, and M. Manfait, Discriminating healthy from tumor and necrosis tissue in rat brain samples by Raman spectral imaging. Biochim. Biophys. Acta **1768**, 2605–2615 (2007).

[37] P. Lasch, W. Haensch, D. Naumann, and M. Diem, Imaging of colorectal adenocarcinoma using FTIR microspectroscopy and cluster analysis. Biochim. Biophys. Acta **1688**, 176–186 (2004).

[38] W. Steller, J. Einenkel, L. C. Horn, U. D. Braumann, H. Binder, R. Salzer, and C. Krafft, Delimitation of squamous cell cervical carcinoma using infrared microspectroscopic imaging. Anal. Bioanal. Chem. **384**, 145–154 (2006).

[39] C. Krafft, S. B. Sobottka, K. D. Geiger, G. Schackert, and R. Salzer, Classification of malignant gliomas by infrared spectroscopic imaging and linear discriminant analysis. Anal. Bioanal. Chem. **387**, 1669–1677 (2007).

[40] C. Krafft, L. Shapoval, S. B. Sobottka, G. Schackert, and R. Salzer, Identification of primary tumors of brain metastases by IR spectroscopic imaging and linear discriminant analysis. Technol. Cancer Res. Treat. **5**, 291–298 (2006).

[41] N. Stone, C. Kendall, N. Shepherd, P. Crow, and H. Barr, Near-infrared Raman spectroscopy for the classification of epithelial pre-cancers and cancers. J. Raman Spectrosc. **33**, 564–573 (2002).

[42] C. Kendall, N. Stone, N. Shephard, K. Geboes, B. Warren, R. Bennet, and H. Barr, Raman spectroscopy, a potential tool for the objective identification

and classification of neoplasia in Barrett's oesophagus. J. Pathol. **200**, 602–609 (2003).
[43] R. A. Shaw, F. B. Guijon, M. Paraskevas, S. L. Ying, and H. H. Mantsch, Infrared spectroscopy of exfoliated cervical cell specimens. Proceed with caution. Anal. Quant. Cytol. Histol. **21**, 292–302 (1999).
[44] D. Rohleder, W. Kiefer, and W. Petrich, Quantitative analysis of serum and serum ultrafiltrate by means of Raman spectroscopy. Analyst **129**, 906–911 (2004).
[45] G. Hosafci, O. Klein, G. Oremek, and W. Mäntele, Clinical chemistry without reagents? An infrared spectroscopic technique for determination of clinical relevant constituents of body fluids. Anal. Bioanal. Chem. **387**, 1815–1822 (2006).
[46] H. Fabian, N. A. N. Thi, M. Eiden, P. Lasch, J. Schmidt, and D. Naumann, Diagnosing benign and malignant lesions in breast tissue sections by using IR microspectroscopy. Biochim. Biophys. Acta **178**, 874–882 (2006).
[47] J. Schmitt, M. Beekes, A. Brauer, T. Udelhoven, P. Lasch, and D. Naumann, Identification of scrapie infection from blood serum by Fourier transform infrared spectroscopy. Anal. Chem. **74**, 3865–3868 (2002).
[48] P. Lasch, M. Beekes, J. Schmitt, and D. Naumann, Detection of preclinical scrapie form serum by infrared spectroscopy and chemometrics. Anal. Bioanal. Chem. **387**, 1791–1800 (2007).
[49] D. C. Fernandez, R. Bhargava, S. M. Hewitt, and I. W. Levin, Infrared spectroscopic imaging for histopathologic recognition. Nat. Biotechnol. **23**, 469–474 (2005).
[50] R. Bhargava, D. C. Fernandez, S. M. Hewitt, and I. W. Levin, High throughput assessment of cells and tissues: Bayesian classification of spectral metrics from infrared vibrational spectroscopic imaging data. Biochem. Biophys. Acta, **1758**, 830–845 (2006).
[51] T. C. Martin, J. Moecks, A. Belooussov, S. Cawthraw, B. Dolenko, M. Eiden, J. von Frese, W. Kohler, J. Schmitt, R. Somorjai, T. Udelhoven, S. Verzakov, and W. Petrich, Classification of signatures of bovine spongiform encephalopathy in serum using infrared spectroscopy. Analyst **129**, 897–901 (2004).
[52] C. Beleites and R. Salzer, Assessing and improving the stability of chemometric models in small sample size situations. Anal. Bioanal. Chem. **390**, 1261–1271 (2008).
[53] B. H. Menze, W. Petrich, and F. A. Hamprecht, Multivariate feature selection and hierarchical classification for infrared spectroscopy: serum based detection of bovine spongiform encephalopathy. Anal. Bioanal. Chem. **387**, 1801–1807 (2007).
[54] R. Bhargava and I. W. Levin, Infrared spectroscopic imaging protocols for high-throughput histopathology. In: M. Diem, J. M. Chalmers, and P. R. Griffiths (eds.) Vibrational Spectroscopy for Medical Diagnosis (John Wiley & Sons Ltd, Chichester, 2008).
[55] M. J. Walsh, M. J. German, M. Singh, H. M. Pollock, A. Hammiche, M. Kyrgious, H. F. Stringfellow, E. Paraskevaidis, P. L. Martin-Hirsch, and F. L. Martin, IR microspectroscopy: potential applications in cervical cancer screening. Cancer Lett. **246**, 1–11 (2007).
[56] R. K. Dukor, Vibrational spectroscopy in the detection of cancer, In: J. M. Chalmers and P. R. Griffiths (eds.) Handbook of Vibrational Spectroscopy (John Wiley & Sons Ltd, Chichester, 2002), 3335–3361.
[57] D. McNaughton, K. Bambery, and B. R. Wood, Spectral histopathology of the human cervix In: M. Diem, J. M. Chalmers, and P. R. Griffiths (eds.) Vibrational Spectroscopy for Medical Diagnosis (John Wiley & Sons Ltd, Chichester, 2008).
[58] P. T. T. Wong, S. Lacelle, M. Sentermann, and F. K. M. Fung, Characterization of the exfoliated cells and tissues from the human endo- and ecto-cervix by FTIR and ATR-FTIR spectroscopy. Biospectrosc. **1**, 357–364 (1995).
[59] B. R. Wood, L. Chiriboga, H. Yee, M. A. Quinn, D. McNaughton, and M. Diem, Fourier transform infrared spectral mapping of the cervical transformation zone and dysplastic epithelium. Gynecol. Oncol. **93**, 59–68 (2004).
[60] J. I. Chang, Y. B. Huang, P. C. Wu, C. C. Chen, S. C. Huang, and Y. H. Tsai, Characterization of human cervical precancerous tissue through the Fourier transform infrared microscopy with mapping method. Gynecol. Oncol. **91**, 577–583 (2003).
[61] N. Stone, C. Kendall, and. H. Barr, Raman spectroscopy as a potential tool for early diagnosis of malignancies in esophageal and bladder tissues. M. Diem, J. M. Chalmers, P. R. Griffiths (eds.) Vibrational Spectroscopy for Medical Diagnosis (John Wiley & Sons Ltd, Chichester, 2008).
[62] C. Krafft and R. Salzer, Neuro-oncological applications of infrared and Raman spectroscopy. In: M. Diem, J. M. Chalmers, and P. R. Griffiths (eds.) Vibrational Spectroscopy for Medical Diagnosis (John Wiley & Sons Ltd, Chichester, 2008).
[63] P. Lasch, M. Beekes, H. Fabian, and D. Naumann, Antemortem identification of transmissible spongiform encephalopathy (TSE) by mid-infrared spectroscopy. In: M. Diem, J. M. Chalmers, and P. R. Griffiths (eds.) Vibrational Spectroscopy for Medical Diagnosis (John Wiley & Sons Ltd, Chichester, 2008).
[64] K. R. Bambery, E. Schültke, B. R. Wood, S. T. Rigley MacDonald, K. Ataelmannan, R. W. Griebel, B. H. J. Juurlink, and D. McNaughton, A Fourier transform infrared microspectroscopic imaging investigation into an animal model exhibiting glioblastoma multiforme. Biochim. Biophys. Acta **1758**, 900–907 (2006).
[65] A. Kretlow, Q. Wang, J. Kneipp, P. Lasch, M. Beekes, L. Miller, and D. Naumann, FTIR microspectroscopy of prion-infected nervous tissue, Biochim. Biophys. Acta **1758**, 948–959 (2006).
[66] M. Beekes, P. Lasch, and D. Naumann, Analytical applications of Fourier transform infrared spectroscopy in microbiology and prion research. Vet. Microbiol. **123**, 305–319 (2007).

[67] J. Kneipp, L. M. Miller, M. Joncic, M. Kittel, P. Lasch, M. Beekes, and D. Naumann, In situ identification of protein structural changes in prion-infected tissue. Biochim. Biophys. Acta **1639**, 152–158 (2003).
[68] P. Lasch, J. Schmitt, M. Beekes, T. Udelhoven, M. Eiden, H. Fabian, W. Petrich, and D. Naumann, Antemortem identification of bovine spongiform encephalopathy from serum using infrared spectroscopy. Anal. Chem. **75**, 6673–6678 (2003).
[69] A. L. Boskey and R. Mendelsohn, Infrared analysis of bone in health and disease. J. Biomed. Opt. **10**(3), 031102 (2005).
[70] A. L. Boskey, E. DiCarlo, E. Paschalis, P. West, and R. Mendelsohn, Comparison of mineral quality and quantity in iliac crest biopsies from high- and low-turnover osteoporosis: an FTIR microspectroscopic investigation. Osteoporos. Int. **16**, 2031–2038 (2005).
[71] D. Faibesh, S. M. Ott, and A. L. Boskey, Mineral changes in osteoporosis. A review. Clin. Orthopod. Relat. Res. **443**, 28–38 (2006).
[72] D. Faibesh, A. Gomes, G. Boivin, I. Binderman, and A. Boskey, Infrared imaging of calcified tissue in bone biopsies from adults with osteomalacia. Bone **36**, 6–12 (2005).
[73] C. P. Tarnowski, M. A. Ignelzi Jr., W. Wang, J. M. Taboas, S. A. Goldstein, and M. D. Morris, Earliest mineral and matrix changes in force-induced musculoskeletal disease as revealed by Raman microspectroscopic imaging. J. Bone Miner. Res. **19**, 64–71 (2004).
[74] N. J. Crane, M. D. Morris, M. A. Ignelzi, and G. Yu, Raman imaging demonstrates FGF2-induced craniosynthesis in mouse calvaria. J. Biomed. Opt. **10**, 031119 (2005).
[75] M. E. Ruppel, D. B. Burr, and L. M. Miller, Chemical makeup of microdamaged bone differs from undamaged bone. Bone **39**, 318–324 (2006).
[76] J. A. Timlin, A. Carden, M. D. Morris, R. M. Rajachar, and D. H. Kohn, Raman spectroscopic imaging markers for fatigue-related microdamage in bovine bone. Anal. Chem. **72**, 2229–2236 (2000).
[77] A. C. Ko, L. P. Choo-Smith, M. Hewko, L. Leonardi, M. G. Sowa, C. C. Dong, P. Williams, and B. Cleghorn, Ex vivo detection and characterization of early dental caries by optical coherence tomography and Raman spectroscopy. J. Biomed. Opt. **10**, 031118 (2005).
[78] D. R. Kodali, D. M. Small, J. Powell, and K. Krishnan, Infrared micro-imaging of atherosclerotic arteries. Appl. Spectrosc. **45**, 1310–1317 (1991).
[79] R. Manoharan, J. J. Baraga, R. P. Rava, R. R. Dasari, M. Fitzmaurice, and M. S. Feld, Biochemical analysis and mapping of atherosclerotic human artery using FTIR microspectroscopy. Atherosclerosis **103**, 181–193 (1993).
[80] H. H. T. Hsu, N. C. Camacho, O. Tawfik, and F. Sun, Induction of calcification in rabbit aortas by high cholesterol diets: roles of calcifiable vesicles in dystrophic calcification. Atherosclerosis **161**, 85–94 (2002).
[81] C. Li, D. Ebenstein, C. Xu, J. Chapman, D. Saloner, J. Rapp, and L. Pruitt, Biochemical characterization of atherosclerotic plaque constituents using FTIR spectroscopy and histology. J. Biomed. Mater. Res. A **64**, 197–206 (2003).
[82] C. S. Colley, S. G. Kazarian, P. D. Weinberg, and M. J. Lever, Spectroscopic imaging of arteries and atherosclerotic plaques. Biopolymers **74**, 328–335 (2004).
[83] S. W. E van de Poll, T. J. Romer, G. J. Puppels, and A. van der Laarse, Imaging of atherosclerosis. Raman spectroscopy of atherosclerosis. J. Cardiovasc. Risk. **9**, 255–261 (2002).
[84] S. W. E. van de Poll, T. C. Bakker Schut, A. van der Laarse, and G. J. Puppels, In situ investigation of the chemical composition of ceroid in human atherosclerosis by Raman spectroscopy. J. Raman Spectrosc. **33**, 544–551 (2002).
[85] S. W. E. van de Poll, D. J. M. Delsing, J. W. Jukema, H. M. G. Princen, L. M. Havekes, G. J. Puppels, and A. van der Laarse, Raman spectroscopic investigation of atorvastatin, amlodipine, and both on atherosclerotic plaque development in APOE*3 Leiden transgenic mice. Atherosclerosis **164**, 65–71 (2002).
[86] S. W. E. van de Poll, K. Kastelijn, T. C. Bakker Schut, G. Pasterkamp, G. J. Puppels, and A. van der Laarse, On-line detection of cholesterol and calcification by catheter based Raman spectroscopy in human atherosclerotic plaque ex vivo. Heart **89**, 1078–1082 (2003).
[87] T. J. Römer, J. F. Brennan, T. C. Schut, R. Wolthuis, R. C. van den Hoogen, J. J. Emeis, A. van der Laarse, A. V. Bruschke, and G. J. Puppels, Raman spectroscopy for quantifying cholesterol in intact coronary artery wall. Atherosclerosis **141**, 117–124 (1998).
[88] C. Palusczkiewicz, W. M. Kwiatek, M. Galka, D. Sobieraj, and E. Wentrup-Byrne, FT-Raman, FTIR spectroscopy and pixe analysis applied to gallstones specimens. Cell. Mol. Biol. **44**, 65–71 (1998).
[89] L. Vitetta, S. P. Best, and A. Sali, Single and multiple cholesterol gallstones and the influence of bacteria. Med. Hypotheses **55**, 502–506 (2000).
[90] J. P. Pestaner, F. G. Mullick, F. B. Johnson, and J. A. Centeno, Calcium oxalate crystals in human pathology. Molecular analysis with the laser Raman microprobe. Arch. Pathol. Lab. Med. **120**, 537–540 (1996).
[91] E. Takasaki, Carbonate in struvite stone detected in Raman spectra compared with infrared spectra and X-ray diffraction. Int. J. Urol. **3**, 27–30 (1996).
[92] V. R. Kodati, G. E. Tomasi, J. L. Turumin, and A. T. Tu, Raman spectroscopic identification of phosphate type kidney stones. Appl. Spectrosc. **45**, 581–583 (1991).
[93] E. H. Yoo, H. J. Oh, and S. Y. Lee, Gallstone analysis using Fourier transform infrared spectroscopy. Clin. Chem. Lab. Med. **46**, 376–381 (2008).
[94] K. Uchiyama, M. Kawai, M. Tani, H. Terasawa, H. Tanimura, and H. Yamaue, Pathogenesis of hepatolithia-

sis based on the analysis of intrahepatic stones. Hepatogastroenterologyy **54**, 1798–1804 (2007).

[95] J. C. Anderson, J. C. Williams Jr., A. P. Evan, K. W. Condon, and A. J. Sommer, Analysis of urinary cacluli using an infrared microspectroscopic surface reflectance imaging technique. Urol. Res. **35**, 41–48 (2007).

[96] A. P. Evan, F. L. Coe, J. E. Lingeman, Y. Shao, B. R. Matlaga, S. C. Kim, S. B. Bledsoe, A. J. Sommer, M. Grynpas, C. L. Phillips, and E. M. Worcester, Renal crystal deposits and histopathology in patients with cystine stones. Kidney Int. **69**, 2227–2235 (2006).

[97] G. Schubert, Stone analysis. Urol. Res. **34**, 146–150 (2006).

[98] O. Kleiner, J. Ramesh, M. Huleihel, B. Cohen, K. Kantarovich, C. Levi, B. Polyak, R. S. Marks, J. Mordechai, Z. Cohen, and S. Mordechai, A comparative study of gallstones from children and adults using FTIR spectroscopy and fluorescence microscopy. BMC Gastroenterol. 2, doi: 10.1186/1471-230X-2-3, (2002).

[99] N. S. Eikje, K. Aizawa, and Y. Ozaki, Vibrational spectroscopy for molecular characterization and diagnosis of benign, premalignant and malignant skin tumors. Biotechnol. Annu. Rev. **11**, 191–225 (2005).

[100] A. Nijssen, T. C. Bakker Schut, F. Heule, P. J. Caspers, D. P. Hayes, M. H. A. Neumann, and G. J. Puppels, Discriminating basal cell carcinoma from its surrounding tissue by Raman spectroscopy. J. Invest. Dermatol. **119**, 64–69 (2002).

[101] A. Tfayli, O. Piot, A. Durlach, P. Bernard, and M. Manfait, Discriminating nevus and melanoma on paraffin-embedded skin biopsies using FTIR microspectroscopy. Biochim. Biophys. Acta, **1724**, 262–269 (2005).

[102] M. Gniadecka, P. A. Philipsen, S. Sigurdsson, S. Wessel, O. F. Nielsen, D. H. Christensen, J. Hercogova, K. Rossen, H. K. Thomsen, R. Gniadecki, L. K. Hansen, and H. C. Wulf, Melanoma diagnosis by Raman spectroscopy and neural networks: structure alteration in proteins and lipids in intact cancer tissue. J. Invest. Dermatol. **122**, 443–449 (2004).

[103] L. M. McIntosh, M. Jackson, H. H. Mantsch, M. Stranc, D. Pilavdzic, and A. N. Crowson, Infrared spectra of basal cell carcinomas are distinct from non-tumor-bearing skin components. J. Invest. Dermatol. **112**, 951–956 (1999).

[104] M. A. Short, H. Lui, D. I. McLean, H. Zeng, and M. X. Chen, Proc. SPIE 6093, 60930E/1-60930E/6 (2006). Preliminary micro-Raman images of normal and malignant human skin cells.

[105] C. A. Lieber and A. Mahadevan-Jansen, Development of a handheld Raman microspectrometer for clinical dermatologic applications. Opt. Exp. **15**, 11874–11882 (2007).

[106] R. A. Shaw and H. H. Mantsch, Infrared spectroscopy in clinical and diagnostic analysis. In: R. A. Meyers (ed.) Encyclopedia of Analytical Chemistry (Wiley & Sons, Chichester, 2000).

[107] C. Petibois and G. Deleris, Chemical mapping of tumor progression by FTIR imaging: towards molecular histopathology. Trends Biotechnol. **24**, 455–462 (2006).

[108] X. Bi, X. Yang, M. P. G. Bostrom, and N. P. Camacho, Fourier transform infrared imaging spectroscopy investigations in the pathogenesis and repair of cartilage. Biochim. Biophys. Acta **1758**, 934–941 (2006).

[109] P. A. West, M. P. G. Bostrom, P. A. Torzilli, and N. P. Camacho, Fourier transform infrared spectral analysis of degenerative cartilage: an infrared fiber-optic probe and imaging study. Appl. Spectrosc. **58**, 376–381 (2004).

[110] C. L. Evans, E. O. Potma, M. Puoris'haag, D. Cote, C. P. Lin, and X. S. Xie, Chemical imaging of tissue in vivo with video-rate coherent anti-Stokes Raman scattering microscopy. Proc. Natl. Acad. Sci. (USA) **102**, 16807–16812 (2005).

